





RESEARCH ARTICLE

Variable histopathology features of neuronal dyslamination in the cerebral neocortex adjacent to epilepsy-associated vascular malformations suggest complex pathogenesis of focal cortical dysplasia ILAE type IIIc

Hajime Miyata¹  | Haruka Kuwashige^{1,2} | Tomokatsu Hori³ | Yuichi Kubota^{4,5}  | Tom Pieper⁶ | Roland Coras⁷  | Ingmar Blümcke⁷  | Yasuji Yoshida¹

¹Department of Neuropathology, Research Institute for Brain and Blood Vessels, Akita Cerebrospinal and Cardiovascular Center, Akita, Japan

²Akita University School of Medicine, Akita, Japan

³Department of Neurosurgery, Medical Corporation Moriyamakai, Moriyama Neurological Center Hospital, Tokyo, Japan

⁴Department of Neurosurgery, Adachi Medical Center, Tokyo Women's Medical University, Tokyo, Japan

⁵Epilepsy Center, TMG Asaka Medical Center, Saitama, Japan

⁶Center for Pediatric Neurology, Neurorehabilitation, and Epileptology, Schoen-Clinic, Vogtareuth, Germany

⁷Department of Neuropathology, University Hospital Erlangen, Friedrich-Alexander University, Erlangen, Germany

Correspondence

Hajime Miyata, Department of Neuropathology, Research Institute for Brain and Blood Vessels, Akita Cerebrospinal and Cardiovascular Center, 6-10 Senshu-Kubota-Machi, Akita City, Akita 010-0874, Japan.
Email: hmiyata@akita-noken.jp

Funding information

Akita Cerebrospinal and Cardiovascular Center

Abstract

Focal cortical dysplasia type IIIc (FCD-IIIc) is histopathologically defined by the International League Against Epilepsy's classification scheme as abnormal cortical organization adjacent to epilepsy-associated vascular malformations (VM). However, the incidence of FCD-IIIc, its pathogenesis, or association with the epileptogenic condition remains to be clarified. We reviewed a retrospective series of surgical brain specimens from 14 epilepsy patients with leptomeningeal angiomatosis of Sturge-Weber syndrome (LMA-SWS; $n = 6$), cerebral cavernous malformations (CCM; $n = 7$), and an arteriovenous malformation (AVM; $n = 1$) to assess the histopathological spectrum of FCD-IIIc patterns in VM. FCD-IIIc was observed in all cases of LMA-SWS and was designated as cortical pseudolaminar sclerosis (CPLS). CPLS showed a common pattern of horizontally organized layer abnormalities, including neuronal cell loss and astrogliosis, either manifesting predominantly in cortical layer (L) 3 extending variably to deeper areas with or without further extension to L2 and/or L4. Another pattern was more localized, targeting mainly L4 with extension to L3 and/or L5. Abnormal cortical layering characterized by a fusion of L2 and L3 or L4–L6 was also noted in two LMA-SWS cases and the AVM case. No horizontal or vertical lamination abnormalities were observed in the specimens adjacent to the CCM, despite the presence of vascular congestion and dilated parenchymal veins in all VM. These findings suggest that FCD-IIIc depends on the type of the VM and developmental timing. We further conclude that FCD-IIIc represents a secondary lesion acquired during pre- and/or perinatal development rather than following a pathomechanism independent of LMA-SWS. Further studies will be necessary to address the selective vulnerability of the developing cerebral neocortex in LMA-SWS, including genetic, encephaloclastic, hemodynamic, or metabolic events.

This is an open access article under the terms of the [Creative Commons Attribution-NonCommercial-NoDerivs](https://creativecommons.org/licenses/by-nc-nd/4.0/) License, which permits use and distribution in any medium, provided the original work is properly cited, the use is non-commercial and no modifications or adaptations are made.

© 2022 The Authors. *Brain Pathology* published by John Wiley & Sons Ltd on behalf of International Society of Neuropathology

KEY WORDS

cerebral neocortex, epilepsy surgery, focal cortical dysplasia, neuron, pathogenesis, vascular malformation

1 | INTRODUCTION

Vascular malformation (VM) is a generic term referring to a group of presumably congenital abnormalities of blood vessels caused by disordered mesodermal differentiation between the third and eighth week of gestation in the developing human embryo [1]. Intracranial VM generally present as focal lesions. They can be clinically asymptomatic or present with spontaneous hemorrhage, including brain parenchymal or subarachnoid hemorrhage or both, and responsible for a wide range of neurological symptoms, including epilepsy in children and young adults.

Intracranial VM commonly encountered in surgical pathology or autopsy includes the following.

- Arteriovenous malformation (AVM).
- Cerebral cavernous malformation (CCM).
- Developmental venous anomaly (DVA).
- Capillary telangiectasia.
- Leptomeningeal angiomatosis of Sturge-Weber syndrome (LMA-SWS).

According to the European Epilepsy Brain Bank, VM is the 5th frequent among seven major histopathological disease categories, comprising only 6.1% of 9523 epilepsy surgery cases [2]. However, the actual prevalence of epilepsy-associated VM may be higher, as it is not uncommon for epilepsy patients with these lesions to be treated in the stroke unit. Among all types of VM, CCM is most frequently associated with epileptic seizures and is commonly encountered in surgical specimens from patients with drug-resistant focal epilepsy [3]. Factors considered to be involved in the epileptogenic mechanisms for VM may include chronic parenchymal iron deposition or siderosis, glial scarring around the VM, and blood-brain barrier dysfunction and subsequent astrocytic albumin uptake [3–5], as well as cortical neuronal dyslamination detected outside the area of ischemia or hemorrhage adjacent to VM [6].

According to the classification of focal cortical dysplasia (FCD) by the International League Against Epilepsy (ILAE), “FCD type III (FCD-III)” refers to an abnormal neocortical organization in association with a principal epileptogenic lesion [6]. FCD-III is further distinguished into four subtypes; i.e., neuronal dyslamination associated with hippocampal sclerosis (FCD type IIIa), neoplasm (IIIb), VM (IIIc), and any other, mostly destructive lesion acquired during early life such as traumatic brain injury, hemorrhage, ischemia, inflammation, or infectious diseases (IIId). Since the inauguration

of this widely accepted classification in 2011, only a limited number of histological studies have addressed the FCD-IIIc subtype [7, 8]. Therefore, not much is known with certainty about the histologic features and pathogenesis of FCD-III. This study aimed primarily to investigate whether or not FCD-IIIc is present in each type of VM and, if present, to describe the histological features of cortical dyslamination. The second aim was to discuss its pathogenic mechanism based on the histological findings, addressing the critical question as to whether FCD-IIIc represents an independent congenital malformation of cortical development or a lesion resulting secondary to the development and pathophysiology of epileptogenic VM.

2 | MATERIALS AND METHODS

Fourteen surgically resected specimens from epilepsy patients with VM (number of male and female patients [M: F], 9:5; median age at surgery, 32.5 years; age range, 2.5–54 years) were retrospectively chosen for this study from archival paraffin blocks. These include tissue from patients with (I) LMA-SWS (M: F, 6:0; median age, 17 years; age range, 2.5–45 years), (II) CCM (M: F, 2:5; median age, 41 years; age range, 22–54 years) and (III) AVM (26 years, M) (Table 1). All patients were sporadic cases with no family history of epilepsy. After detailed presurgical epileptological evaluation assessing seizure semiology, MRI and other neuroimaging findings, video-scalp electroencephalography (EEG) monitoring, and electrocorticography (ECoG) by subdural grid electrodes, all patients underwent *en bloc* resection or lobectomy, but not lesionectomy alone, including the whole VM and surrounding brain tissue containing at least more than two gyri. Postsurgical seizure outcome was evaluated two years after surgical intervention and scored according to the Engel classification [9]. The size and location of each VM were evaluated in the fixed resection specimens. Five-micrometer-thick sections were stained with Luxol fast blue (LFB)-hematoxylin and eosin (HE), Elastica-Masson, and Prussian blue. Adjacent serial sections were subjected to panels of immunohistochemistry performed by the polymer-immunocomplex method using a BOND Polymer Refine Detection with the 3-3' diaminobenzidine (Leica Biosystems, Newcastle Upon Tyne, UK) as the chromogen and hematoxylin as the counterstain, using an automated IHC stainer Leica BOND MAX (Leica Biosystems, Tokyo, Japan). Primary antibodies used in this study include anti-neuronal nuclear antigen (NeuN)

TABLE 1 Summary of clinicopathological findings

Lesion type and case #	Age at surgery (y)	Sex	Seizure onset age (y)	Engel class	Location and size of the vascular lesion resected	CPLS, HN, and MAP1b-positive neurons						Indistinct neuronal layering	Other lesions										
						L2		L3			L4			L5	L6								
						S	D	S	M	D	S			D									
LMA-SWS 1	44	M	na	II	Lt whole P-O, 60 mm x 50 mm x 60 mm			■	■	■													
2	2.5	M	0.6	IA	Rt T-P-O, posterior quadrantectomy					■										L2-L3, L4-L6 L2-L4			
3	16	M	10	IA	Lt P, lobectomy			■	■	■											L3-L4, L4-L6 No-HS		
4	45	M	na	IA	T, lobectomy								■									HS type 1	
5	17	M	na	IA	O, lobectomy								■										
6	6	M	2	na	Lt F-P, lobectomy			■	■	■													
Median age			17	2																			
CCM 7	41	M	na	II	Lt T CTX, 10 mm (d)																		
8	22	F	na	I	Lt anterior cingulate cortex, 5 mm (d)																		
9	45	F	20	I	Lt F CTX-WM, 18 mm x 15 mm x 12 mm																		
10	54	F	53	I	Lt T pole CTX-WM, 10 mm (d)																		
11	28	M	25	IA	Lt T base CTX, less than 10 mm (d)																		
12	53	F	34	I	Lt O CTX, 13 mm x 7 mm x 15 mm																		
13	37	F	20	I	Rt T CTX-WM, 15 mm x 19 mm x 13 mm																		
Median age			41	25																			
AVM 14	26	M	25	I	Lt T WM-CTX, 11 mm x 10 mm x 20 mm																		L2-L6 SHN

Note: Subdivision of layers: S, shallow; M, middle; D, deep zone of a given layer. Black, orange, and green bars indicate the distributions of CPLS, HN, and MAP1b-expressing neurons, respectively. HN is defined as pyramidal neurons existing outside L5 and larger than those in L5 with a strong cytoplasmic expression of NF-H and/or MAP2.

Abbreviations: AVM, arteriovenous malformation; CCM, cerebral cavernous malformation; CPLS, cortical pseudolaminar sclerosis; CTX, neocortex; d, diameter; F, frontal; HN, hypertrophic neuron; HS, hippocampal sclerosis; L, layer; LMA-SWS, leptomeningeal angiomatosis of Sturge-Weber syndrome; Lt, left; na, data not available; O, occipital; P, parietal; Rt, right; SHN, single heterotopic neurons in white matter; T, temporal; WM, white matter; y, years.



FIGURE 1 Leptomeningeal angiomatosis and cortical calcifications in SWS. (A–C) This surgical specimen was obtained from a 44-year-old male epilepsy patient with SWS (case 1 in Table 1). (A) A collection of dilated and congestive venous vessels in the subarachnoid space, i.e., leptomeningeal angiomatosis (LMA), and typical cortical calcifications of tram-track pattern mainly affecting layer (L) 2 and L4 (asterisks). LFB-HE staining. (B) Parenchymal veins in the white matter (arrows) are also significantly dilated and congested. Calcifications are accentuated in the superficial cortical area (asterisk). Elastica-Masson staining. (C) Conspicuous string-like, vertically oriented linear calcifications along the microvessels are accentuated in L2–L4. Larger plaque-like calcifications are also accumulating mainly in L4 (asterisk). Immunohistochemistry for NeuN with hematoxylin counterstain. These features suggest the underlying hemodynamic abnormalities in the brain parenchyma and cortical areas where lesions are more likely to occur in patients with SWS

(clone A60, dilution 1:400, Chemicon, Temecula, CA, USA), anti-microtubule-associated protein 2 (MAP2) (clone HM-2, dilution 1:6000, Abcam, Tokyo, Japan),

anti-microtubule-associated protein 1B (MAP1B) (clone 3G5, dilution 1:3000, Thermo Fisher Scientific, Cheshire, UK), anti-non-phosphorylated neurofilament

H (NF-H) (clone SMI32, dilution 1:400, BioLegend, San Diego, CA, USA), anti-GFAP (clone 6F2, dilution 1:400, Dako, Glostrup, Denmark), anti-GFAP (clone GA5, dilution 'ready-to-use', Leica Biosystems, Newcastle Upon Tyne, UK), anti-calbindin D-28k (clone CB300, dilution 1:200, Swant, Burgdorf, Switzerland), anti-CD68 (mouse monoclonal, clone KP1, Dako, Glostrup, Denmark, dilution 1:200), anti-HLA-DP, DQ, DR antigen (mouse monoclonal, clone CR3/43, Dako, Glostrup, Denmark, dilution 1:2000), anti-ferritin heavy chain (rabbit monoclonal, clone EPR3005Y, Abcam, Japan, dilution 1:100), and anti-BRAF V600E (rabbit monoclonal, clone RM8, Dianova, Germany, dilution 1:400). Immunostaining with the omission of primary antibodies was used as a negative control. Neuronal dyslamination was evaluated in the neocortex, outside the ischemic or hemorrhagic areas, and areas free of iron deposition evaluated with Prussian blue staining with no or subtle, if any, calcification adjacent to VM. This study was approved by the ethics committee at the authors' institutions and was carried out following the Declaration of Helsinki (as revised in Brazil 2013), with each patient's or relevant person's informed consent and preserving the patient's anonymity.

3 | RESULTS

In patients with LMA-SWS, dilated venous vessels aggregated in the subarachnoid space, i.e., LMA, and typical cortical calcifications of tram-track patterns mainly affected the cortical layers L2 and L4 (Figure 1A). Patterns and extent of calcifications were variable, either confined to L2 and L3 (Figure 1B) or affecting mainly L4 (Figure 1C). Calcifications were observed in all but one case of LMA-SWS (Table 1). Numerous small calcospherites were often accentuated in the wall of capillaries or postcapillary venules. Vascular dilatation and congestion were noted in both meningeal angiomatosis (Figure 1A) and parenchymal veins of the white matter (Figure 1B). In all six patients with LMA-SWS, neuronal dyslamination was observed by NeuN immunohistochemistry in the neocortex with no or minimum calcification, i.e., compatible with FCD-IIIc. This FCD-IIIc pattern was characterized by horizontally oriented neuronal cell loss and astrogliosis of varying thickness and depth, i.e., parallel to the pial surface (Table 1). There were no cystic cavities, macrophages, inflammatory cell infiltrates, or neovascularizations within or around these lesions, and the term 'cortical pseudolaminar sclerosis (CPLS)' will be further used in the present study to discriminate this lesion pattern from 'cortical laminar necrosis' seen in hypoxic-ischemic injuries. We observed two patterns of CPLS in our case series. The more frequent pattern was observed in four patients (cases 1, 3, 5, 6), compromising the shallower zone of L3 extending variably downward to its middle and deeper areas, with

or without further extension to neighboring L2, L4, or both (Figure 2A–C). Another pattern was seen in three patients (cases 1, 2, 4) in which the CPLS targeted mainly L4 and with a presumable extension to the deepest zone of L3 or shallowest zone of L5 (Figure 3A–E). However, it was somewhat inconclusive whether L3 and/or L5 were involved or spared by the lesion because of the layer's indistinct borders. Regardless of the presence or absence of CPLS, MAP2-positive hypertrophic pyramidal neurons outside L5 were observed in all patients with LMA-SWS with variable cell densities (Figure 3D,I), and MAP1B-positive neurons were observed across the depth of L2 and L3 (Figures 2C–G and 3E,J). CPLS was accompanied by the accumulation of HLA-DP, DQ, DR-positive activated microglial cells of varying density (Figure 4A,D). However, iron depositions by Prussian blue staining were not observed, including the areas of LMA and CPLS (Figure 4B,E). The expression of CD68 was not accentuated in the CPLS. Ferritin heavy chain immunoreactivity was confined to oligodendrocytes in both cortex and white matter and not in other cellular components, including astrocytes, microglial cells, and neurons (Figure 4C,F).

Furthermore, loss of cortical lamination was also observed regardless of the presence or absence of CPLS in two cases. In case 1 (44 years old), the cortex showing the deeper pattern of CPLS described above was thinner than the neighboring normal-appearing neocortex, and the distinction between L2 and L3, and L4 through L6 remained ambiguous on LFB-HE staining and NeuN immunohistochemistry (data not shown). The same region also revealed loss of neuronal profiles immunoreactive for NF-H and MAP1B, or MAP2-positive hypertrophic neurons. A similar loss of cortical lamination was observed in case 2 (2.5 years old); i.e., the cortex affected by the deeper pattern CPLS showed indistinct layering between L3 and L4 and from L4 through L6 (Figure 3A–C) compared to adjacent normal-appearing hexalaminar neocortex (Figure 3F–H). The expression of NF-H was faint and confined to a few slender pyramidal neurons scattered in the deeper zone of L3 and L5 (Figure 3B), and MAP2 immunohistochemistry revealed scattered hypertrophic pyramidal neurons in the deepest zone of L3 (Figure 3D). In addition, abnormal organization of L2 and L3 was also observed in the cortex even without CPLS in case 1; i.e., most neurons in the presumed L2 area showed a pyramidal shape being larger than normal L2 granular neurons (Figure 5A,D), and some of them showed cytoplasmic accumulation of NF-H and/or MAP2 (Figure 5B,C), resulting in an ambiguous border between L2 and L3.

The feature of polymicrogyria was not observed in any of the LMA-SWS cases in the present study.

In all patients with CCM, well-circumscribed, multilobulated, "mulberry"-shaped lesions, measuring 5 to 19 mm in maximal dimension, with rusty orange-brown discoloration localized mainly in the cerebral cortex

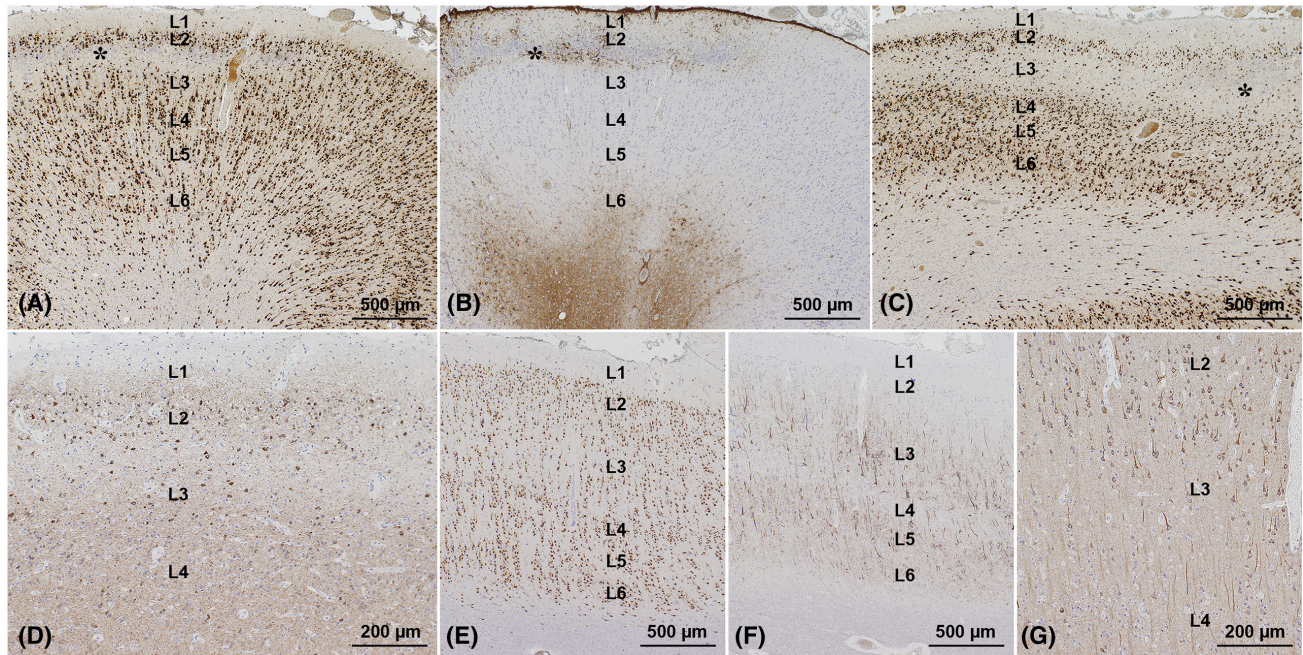


FIGURE 2 FCD-IIIc with CPLS in superficial cortical areas. (A–D) The resection specimen was obtained from a 6-year-old epileptic male with SWS (case 6 in Table 1). (A) A horizontal zone of neuronal loss involving the deeper layer (L) 2 and superficial L3 (asterisk). Immunohistochemistry for NeuN with hematoxylin counterstain. (B) The lesion shown in panel A is accompanied by GFAP-immunoreactive astroglia and termed, therefore, cortical pseudolaminar sclerosis (CPLS). This lesion pattern is reminiscent of temporal lobe sclerosis described in epilepsy patients with hippocampal sclerosis. (C) A more extensive lesion affecting the entire L3, extending partially to L2 and L4 (asterisk). NeuN immunohistochemistry. (D) The remaining neurons in L2 and L3 are immunoreactive for MAP1b. (E–G) The resection specimen from case 1. (E) NeuN immunohistochemistry shows a normal 6-layered neuronal arrangement in the parietal cortex. One may argue that the microcolumnar arrangement of neurons in particularly thick L3 represents a structural abnormality; however, this is a standard feature for the normal parietal cortex. (F) In addition, immunohistochemistry for non-phosphorylated neurofilament H (NF-H) in the same area in panel E demonstrates NF-H positive neurons in L3, L5, and L6, also indicating a normally developed layered cortical organization. (G) A magnified view of the area including L2–L4 in panels E and F demonstrating MAP1b immunoreactive neurons in L2 to shallower L3

with or without extension to the underlying white matter (Table 1). Microscopically, CCM consisted of back-to-back thin-walled, irregularly dilated venous vessels without intervening brain parenchyma and accompanied by hemosiderin deposition. The cerebral cortex with iron deposition showed moderate to marked neuronal loss and astroglia. Prussian blue staining and ferritin heavy chain immunohistochemistry confirmed marked cortical Fe^{3+} depositions, which was also seen in reactive astrocytes, macrophage/microglial cells, as well as in a proportion of neurons (Figure 4G,H). In contrast, ferritin expression in the Prussian blue-defined Fe^{3+} -free area remote from the CCM was also confined to oligodendrocytes in both cerebral cortex and white matter (Figure 4I). Of note, cortical dyslamination was never observed in iron-free areas examined. Intriguingly, in case 12, having 19 years history of intractable focal epilepsy, a focal neocortical area adjacent to CCM in the occipital lobe convexity identified as the seizure onset zone by ECoG was histologically free from hemosiderin or iron deposition, and cortical neurons were well preserved showing normal hexalaminar structure consistent with Brodmann area 18 and 19. However, in five patients, MAP2-positive hypertrophic neurons were observed in L3.

In the case of AVM, the nidus of abnormally-dilated malformed vessels with intervening brain parenchyma was found mainly in the superficial subcortical white matter (Figure 6A). Some of these abnormal vessels showed obstructive changes, and a focal hemosiderin and iron deposition was observed in the periphery of the nidus. Adjacent to this VM, i.e., outside the nidus, where no iron deposition or ischemic change was observed, the cortex was thinner with loss of its characteristic cortical lamination except for L1. This pattern was most evident when using NeuN immunohistochemistry (Figure 6B). NF-H immunohistochemistry in the same area demonstrated an aberrantly layered cortical structure with overall weak NF-H expression (Figure 6C) compared to the structurally normal-appearing cortex (Figure 6D,E), and the border between L2 and L3 was still ambiguous because of the presence of large hypertrophic pyramidal neurons showing loss of neuronal polarity and lack of granular neurons in the putative L2 to shallower L3 (Figure 6F–I). Excess of single heterotopic neurons ($36/\text{mm}^2$) was observed in the cerebral subcortical white matter between the malformed vessels (Figure 6J). Most of them showed well-differentiated pyramidal and occasional polymorphic shapes, equal or larger than those in L5 and L6, and none

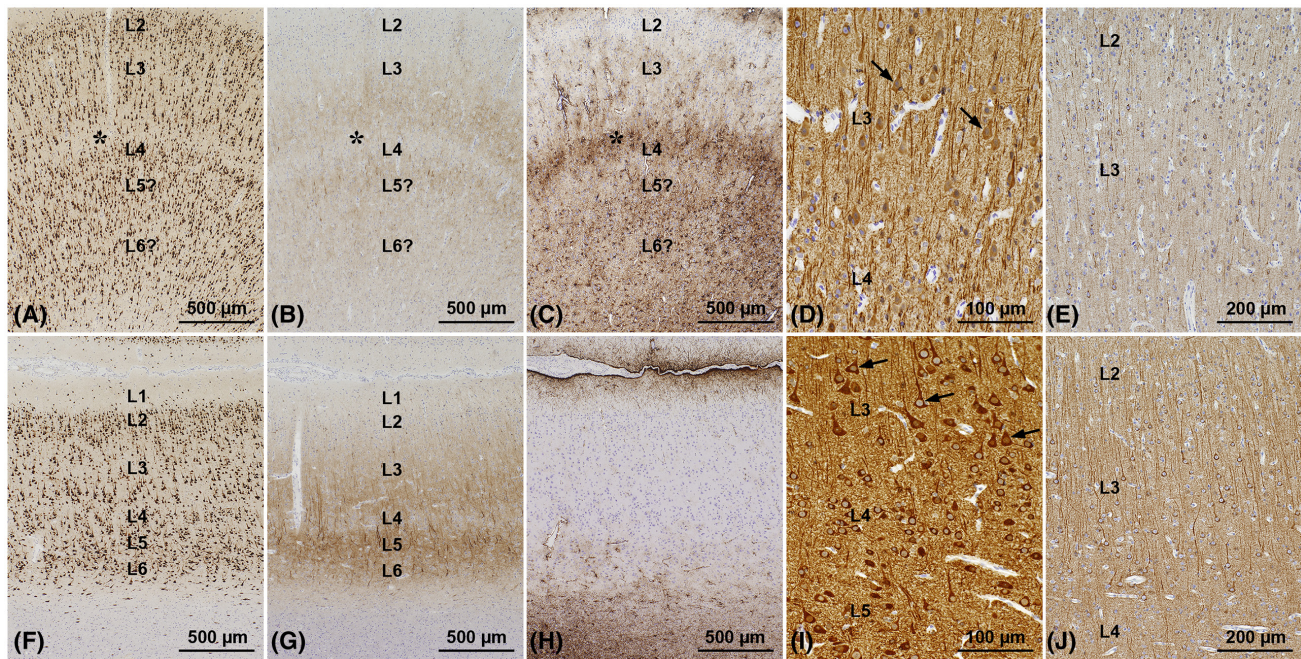


FIGURE 3 FCD-IIIc with CPLS in deeper cortical areas. The resection specimen from a 2.5-year-old epileptic male with SWS (case 2 in Table 1) showing FCD-IIIc involving layer (L) 3 to L6 with CPLS in the deeper cortical areas (A–E) compared to normal-appearing, although thin, hexalaminar neocortex adjacent to this FCD-IIIc on the same specimen (F–J). (A) Neuronal cell loss is evident, affecting the putative deepest L3 and shallower L4 (asterisk). In addition, the separations between L3 and L4, L5, and L6 are uncertain. For comparison, see panel F taken at the same magnification from the adjacent cortex of the same specimen showing a structurally normal-appearing neocortex. NeuN immunohistochemistry with hematoxylin counterstain. (B) Faint NF-H expression is observed in deeper L3, L5, and L6, and the border between L3 and L4 is uncertain because of the CPLS (asterisk). For comparison, see panel G showing stronger NF-H immunoreactivities in L3, L5, and L6. (C) The pseudolaminar neuronal loss shown in panels A and B is accompanied by significant GFAP-positive astrogliosis (asterisk). For comparison, see panel H showing Chaslin's gliosis in L1 only. (D) MAP2-positive hypertrophic pyramidal neurons are scattered in L3 (arrows). By contrast, most neurons in the structurally normal-appearing neocortex are more strongly immunoreactive for MAP2 in their cytoplasm, as shown in panel I, and neurons in L3 are larger than those in L5, a feature characterizing hypertrophic neurons (arrows in I). Panels D and I represent magnified views of L3 and L4 shown in panels A–C and L3–L5 shown in panels F–H, respectively. (E) Most pyramidal neurons in L3 are weakly immunoreactive for MAP1b in FCD-IIIc than the adjacent neocortex shown in panel J. Panels E and J represent magnified views of L2 and L3 shown in panels A–C and L2–L4 shown in panels F–H, respectively

of them were immunoreactive for MAP1b and calbindin D-28k. No immunoreactivity for BRAF V600E was observed in the AVM and surrounding brain parenchyma, while the antibody RM8 revealed mutant cells in ganglioglioma with genetically-confirmed *BRAF* V600E used as a positive control (data not shown). Sanger sequencing of DNA obtained from paraffin-embedded tissue did not detect *BRAF* V600E in the AVM lesion.

In all cases examined in the present study, neither dysmorphic neurons nor balloon cells were observed. Vascular congestion was observed in all VM and dilated parenchymal veins in the adjacent white matter.

4 | DISCUSSION

We identified and histopathologically described different patterns of cortical layer abnormalities, i.e., FCD ILAE type IIIc adjacent to epilepsy-associated LMA-SWS and AVM. Intriguingly, we did not observe FCD-IIIc in any of the studied cases with CCM.

4.1 | Pathogenic considerations of FCD-IIIc associated with LMA-SWS

SWS is a rare sporadic congenital neurocutaneous disorder, characterized by a facial port-wine stain in the distribution of the ophthalmic branch of the trigeminal nerve, ipsilateral LMA, epilepsy, and others [10], affecting both sexes with a slight male predominance [11, 12]. A somatic activating mutation in *GNAQ* has been identified in most patients with SWS, using the lesions from either brain tissue or skin with a port-wine stain [10]. The median age at seizure onset in our LMA-SWS cases was two years and much younger than CCM (25 years) and the AVM (25 years; Table 1). This clinical data are in line with the fact that seizure onset age in SWS is generally young, ranging from birth to young adult, and most patients (75%) have seizure onset before one year [11], suggesting the early intrauterine formation of LMA-SWS in the developing brain. In addition, a rare prenatal diagnosis of SWS at 33 gestational weeks has been reported by fetal neurosonogram and MRI demonstrating

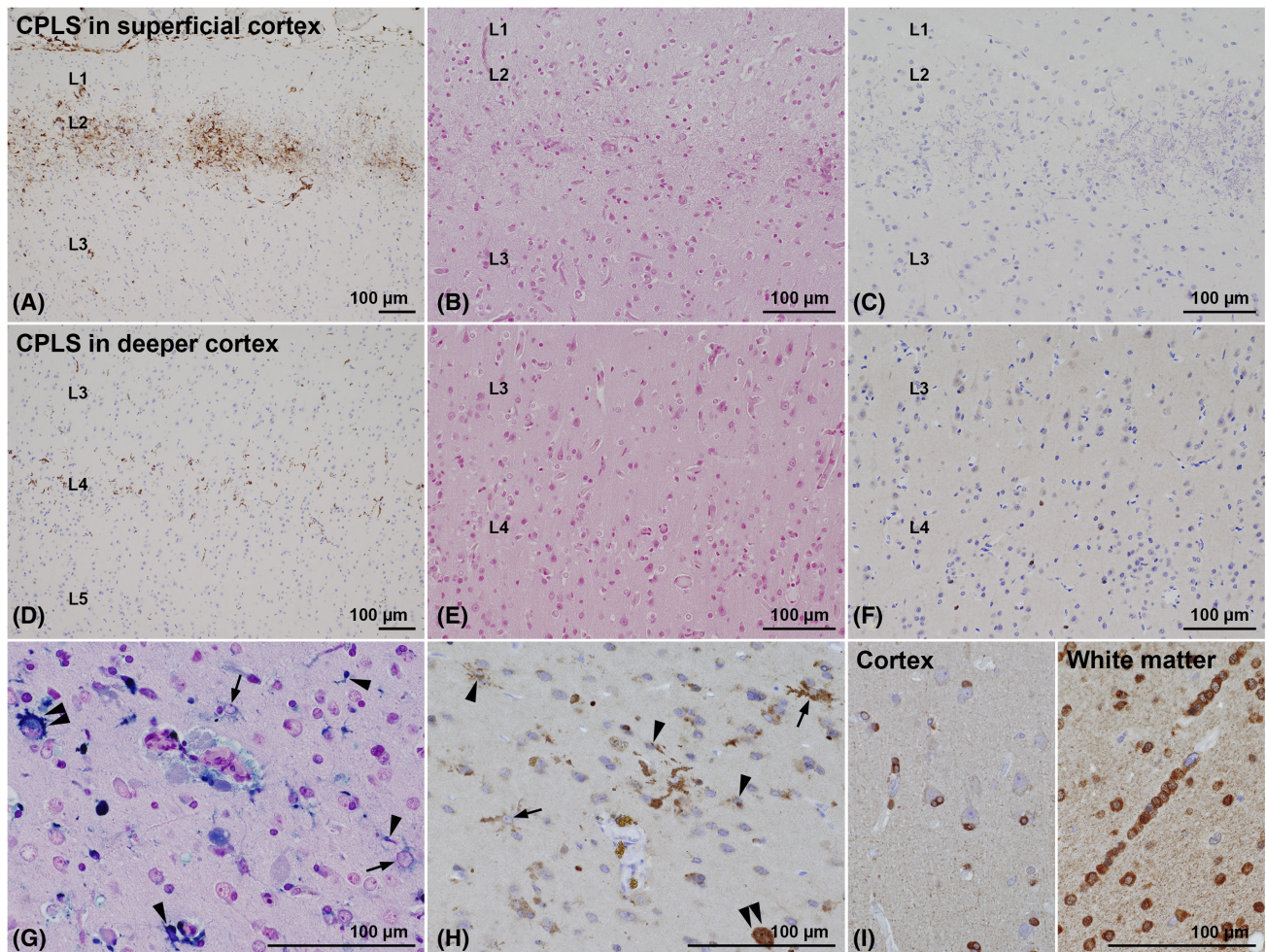


FIGURE 4 Histological and immunohistochemical findings on iron metabolism. (A–C) The resection specimen obtained from a 2-year-old epileptic male with LMA-SWS (case 6 in [Table 1](#)). (D–F) The resection specimen obtained from a 2.5-year-old epileptic male with LMA-SWS (case 2 in [Table 1](#)). (A, D) Lesions of cortical pseudolaminar sclerosis (CPLS) in the superficial and deeper cortex are accompanied by the accumulation of HLA-DP, DQ, DR-positive activated microglial cells of varying density. (B, E) No obvious Fe^{3+} depositions by Prussian blue staining are observed throughout the specimens examined, including the CPLS. (C, F) Ferritin expression in the cortex with CPLS is confined to a small number of oligodendrocytes. (G–I) The resection specimen obtained from a 37-year-old epileptic female with CCM (case 13 in [Table 1](#)). (G) Prussian blue staining in the cerebral cortex with hemosiderin depositions adjacent to CCM demonstrating the presence of Fe^{3+} in reactive astrocytes (arrows), microglial cells (arrowheads), and a proportion of neurons (double arrowheads). (H) Immunohistochemistry for ferritin heavy chain in the same area in panel A demonstrating immunoreactivities in reactive astrocytes (arrows), microglial cells (arrowheads), and a proportion of neurons (double arrowheads). (I) Ferritin expression in the Prussian blue-defined Fe^{3+} -free area remote from the vascular malformations is confined to oligodendrocytes in the cerebral cortex and white matter. Scale bars in all panels indicate 100 μm

gyriform calcification, focal atrophy, abnormal underlying white matter, and a feature of polymicrogyria [13]. Polymicrogyria has been histologically observed also in surgical specimens from patients with LMA-SWS in another study [14], although it was not found in any of our cases. However, these observations indicate that a putative encephaloclastic pathomechanism is associated with LMA-SWS and which dates back to the second trimester undergoing cerebral cortical development by a series of overlapping processes including, e.g., proliferation of matrix cells in the ventricular and subventricular zones, differentiation of neuroblasts and glioblasts, migration of neuroblasts toward the cortical plate, and cortical organization and maturation [15].

Cortical neuronal dyslamination observed in our LMA-SWS cases was mainly attributed to CPLS. Here, we propose a generic term ‘cortical pseudolaminar sclerosis (CPLS)’ to describe a group of such cortical lesions in epilepsy patients characterized histologically by neuronal cell loss and astrogliosis of varying thickness and depth and organized parallel to the pial surface. The absence of significant calcification or a few, if any, calcospherites on the wall of microvessels within CPLS suggests that neuronal loss and gliosis precede the calcification. Of note, CPLS affecting the shallower cortex with MAP1B expression in the remaining L2 neurons is a reminiscence of the lesion described as temporal lobe sclerosis (TLS), a variant classified as FCD-IIIa, and

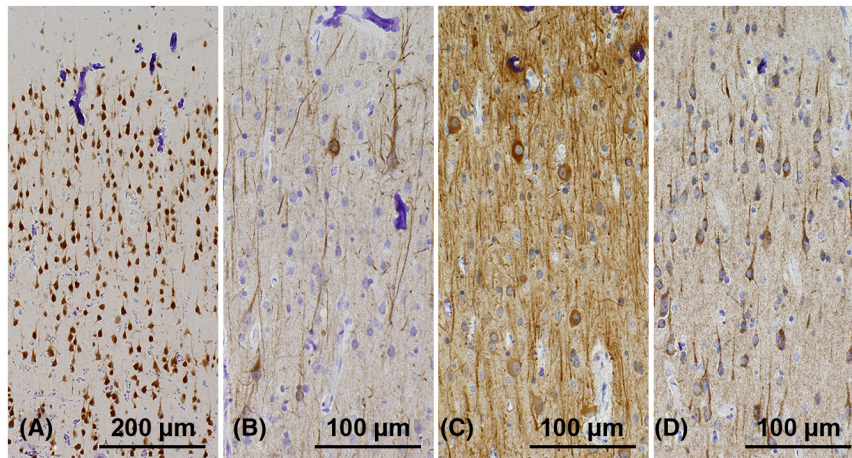


FIGURE 5 Abnormal organization of cortical layers L2 and L3 even without CPLS in SWS. The cerebral cortex without CPLS taken from case 1 (A–D, Table 1, and Figure 1). (A) Only a few neurons can be recognized as granular, whereas many show a pyramidal shape. In addition, the border between layer (L) 2 and L3 is blurred. L1 is presented at the upper margin. NeuN immunohistochemistry with hematoxylin counterstain. Panels B–D represent magnified views from the same region shown in panel A, including the presumed border between L2 and shallower L3. Some pyramidal neurons show accumulation of NF-H (B) and/or MAP2 (C) in their cytoplasm. (D) Many pyramidal neurons are immunoreactive for MAPIb

observed in the temporal neocortex in about 10% of patients with temporal lobe epilepsy (TLE) and hippocampal sclerosis [16]. TLS has never been reported in TLE patients without hippocampal sclerosis nor patients with other epileptogenic and non-epileptogenic brain lesions. Accordingly, we report for the first time that shallower CPLS of varying thickness, the lesion pattern similar to TLS, frequently occurs in the cerebral cortex adjacent to LMA-SWS. Although unraveling the pathogenesis of CPLS as well as TLS is a scope of future investigation, the fact that the shallower zone of the cerebral cortex is vulnerable to hypoglycemia in both humans [17] and animal models [18] may suggest a possible role of localized relative glucose deficiency caused by a supply-demand gap during repetitive hyperexcitation the pathogenesis of CPLS, which needs to be further studied and pathophysiologically confirmed.

On the contrary, the deeper CPLS involving L4 was observed in three of our 6 LMA-SWS cases. This lesion pattern is almost identical to FCD-IIIc described in patients with early-onset posterior quadrant epilepsy who have histories of perinatal transient hypoxic-ischemic insults. Their cortices are histologically characterized by neuronal loss in L4 in the occipital lobe [19, 20]. Thus, perinatal hypoxia/ischemia and/or birth trauma might play a role as acquired (i.e., an extrinsic) pathogenesis in FCD-IIIc. Although our patients with LMA-SWS did not reveal such clinical history, we hypothesize a focal intracranial hypoxic-ischemic pathomechanism to play a role in the manifestation of FCD type IIIc at L4, i.e., caused by the altered hemodynamics associated with venous stasis caused by LMA-SWS.

Another potential mechanism of neuronal dysfunction and cell death is increased oxidative stress from free radicals unleashed through the redox activity of excess

iron (Fe). Iron has been implicated in causing neuronal damage in several neurodegenerative diseases, such as Alzheimer's disease and Parkinson's disease [21]. A recent study has suggested that chronic neuronal iron uptake plays a role in neuronal dysfunction and loss in epilepsy-associated hippocampal sclerosis [22]. Although FCD-IIIc was evaluated in the area free of Fe^{3+} deposition by Prussian blue staining in the present study, this observation may exclude the possibility that excess iron was involved in the pathogenesis of CPLS. Specifically, Prussian blue staining may not detect small amounts of protein-bound, ferric iron (Fe^{3+}) and is, therefore, unable to identify protein-unbound, soluble, ferrous iron (Fe^{2+}) that mainly contributes to the Fenton reaction. However, our results indicate that (1) neuronal loss was confined to areas with positive Prussian blue staining in all CCM cases and the AVM case, and to the intervening cortex of AVM, and that (2) CPLS was observed only in LMA-SWS cases. These results militate against seizure-mediated impaired iron metabolism in hippocampal sclerosis or in the pathogenesis of CPLS.

Loss of cortical lamination by NeuN immunohistochemistry was another feature of FCD-IIIc. This feature, observed regardless of the presence or absence of CPLS, seems to be attributed to either abundant larger pyramidal neurons replacing the presumed L2 with lack of normal granular neurons in the CPLS-free cortex or the slender pyramidal neurons in L3 and L5 showing down-regulation of neuronal cytoskeletal protein expression, possibly caused by chronic ischemia, in the cortex affected by the deeper type CPLS.

Interestingly, male predominance has been demonstrated in the previous clinicopathological reports of FCD-IIIc [20], SWS-associated FCD-IIIc [14], and in our study, that is of unknown reason and significance.

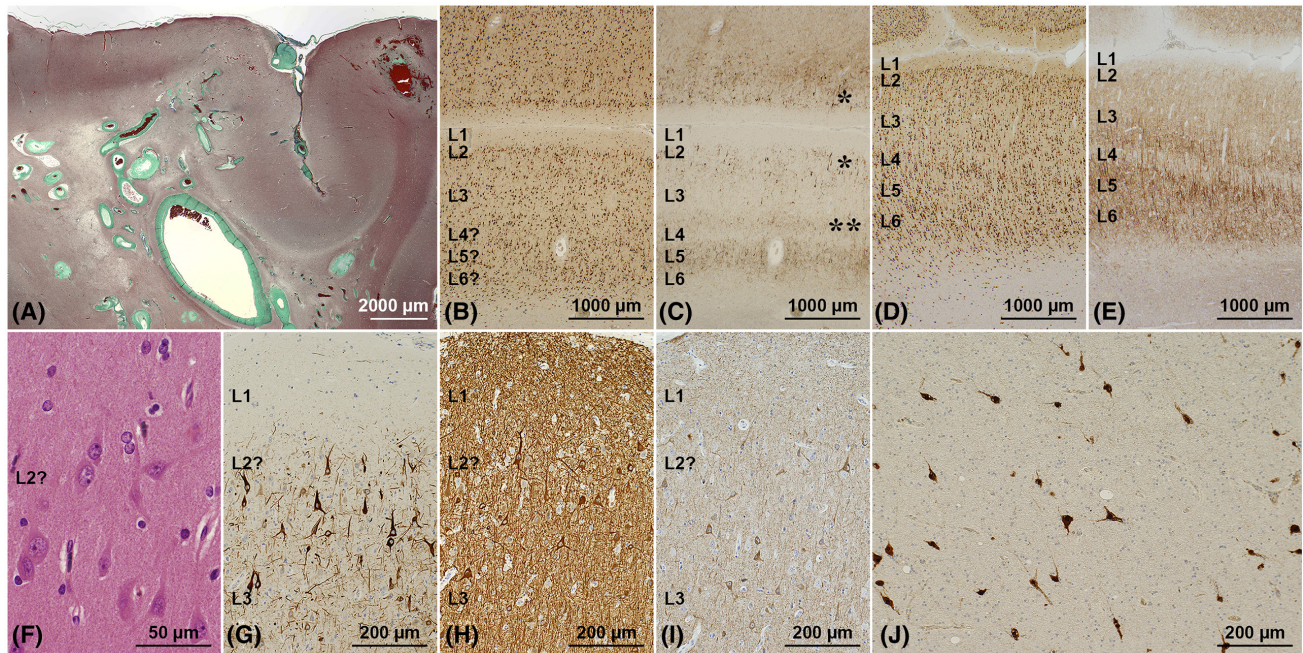


FIGURE 6 FCD-IIIc associated with AVM. (A) The resection specimen was obtained from a 26-year-old male epilepsy patient with AVM (case 14 in Table 1) showing a collection of irregularly dilated malformed vessels located mainly in the subcortical white matter, i.e., a nidus. Elastic-Masson staining. (B) In the cortex adjacent to the AVM, the borders between layers (L) 2 to L6 are indistinct and blurred, compatible with FCD-IIIc. NeuN immunohistochemistry with hematoxylin counterstain. (C) Immunohistochemistry for non-phosphorylated neurofilament H (NF-H) in the same area shown in panel B, demonstrating overall weak expression of NF-H (compared to panel E) with few neurons accumulating NF-H in L2 to shallower L3 (single asterisks), deep L3 (double asterisks), and L5, suggesting a preexisting hexalaminar organization of the neocortex. (D) NeuN immunohistochemistry showing a normal 6-layered neuronal arrangement in the cerebral cortex in the same specimen but remote from the AVM, compared to panel B. (E) NF-H expression is accentuated in L3, L5, and L6 in the same area shown in panel D. Of note, the FCD-IIIc cortex presented in panels B, C is thinner than the structurally normal-appearing cortex shown in panels D, E. (F) A magnified view of L2 within FCD-IIIc, presented in panels B and C, demonstrating large pyramidal neurons, loss of neuronal polarity, and lack of granular neurons. LFB-HE staining. (G) A magnified view of the area including L1 to L3, shown in panels B and C, demonstrating large pyramidal neurons with strong immunoreactivity for NF-H, loss of neuronal polarity, and dystrophic neurites in L2 and shallower L3. (H) Large pyramidal neurons with strong immunoreactivity for MAP2 observed in the same area presented in panel G. (I) Large pyramidal neurons with immunoreactivity for MAP1b observed in the same area shown in panels G and H, and consistent with hypertrophic neurons. (J) Abundant heterotopic neurons are observed in the subcortical white matter in between malformed vessels

Although the pathogenesis of SWS-associated FCD-IIIc is yet to be elucidated, it is likely to be complex and includes altered developmental, encephaloclastic, hemodynamic, and metabolic mechanisms associated with the formation of LMA and seizure activity. Such a complex mechanism likely results in secondary tissue injury and adaptation as represented by the selective vulnerability in the developing cerebral cortex. Secondary tissue injury may not be classified as cortical malformation with a pathomechanism independent of the principal lesion. Despite these considerations, the designation of CPLS as FCD-IIIc would still be compatible with the current FCD classification scheme proposed by the ILAE, as the term ‘dysplasia’ is defined as a morphologic anomaly arising either prenatally or postnatally from dynamic or ongoing alteration of cellular constitution, tissue organization or function within a specific organ or a specific tissue type [23] and ‘abnormal histogenesis’ is used synonymously for ‘dysplasia.’

4.2 | FCD-IIIc is not associated with CCM

CCM, also known as cavernous angioma, cavernous hemangioma, and cavernoma, is the second most common type of VM after DVA [24], accounting for approximately 5% to 15% of all vascular abnormalities in the central nervous system [25]. At least three genes, including *CCM1/KRIT1*, *CCM2/MGC4607*, and *CCM3/PDCD10*, have been identified as responsible for familial CCMs [24, 26]. However, the majority (80%) of CCM are sporadic cases [27], and single somatic mutations in *CCM1* and *CCM2* have also been identified even in sporadic CCM lesions [28]. Familial CCM lesions tend to be multiple, whereas most sporadic CCM is single lesions.

CCM has also been considered congenital. However, they are, in fact, dynamic rather than static lesions because progressive growth of the lesion and repetitive hemorrhages, as well as de novo formation of CCM with or without previous irradiation, can be observed [29]. Most patients with CCM present in their 30s to 50s, with

seizures as the most common presenting symptom for supratentorial lesions [3, 24, 25]. Furthermore, CCM is rarely detected in the fetal and neonatal periods [30, 31]. Given that the median age at seizure onset in our CCM cases was 25 years, and CCM are low flow focal small vascular lesions unlike relatively large LMA-SWS, it is most likely that CCM develops in the postnatal brains, and the associated altered parenchymal hemodynamics does not have any effects on cerebral cortical structure in the postnatal later developing brain or mature cerebral cortex outside the area of hemosiderin deposition. In the present study, cortical dyslamination was never identified in our CCM cases, hence 'No FCD' [32], even in the area of ECoG-defined seizure onset zone (case 12), which is consistent with the previous study indicating a low overall incidence (2 of 47 cases; 4.3%) of CCM-associated cortical dyslamination, being detected only in patients with multiple CCM (2 of 7 cases; 28.6%) but not in patients with single CCM (0 of 40 cases; 0%) [8]. These results suggest that CCM-associated FCD-IIIc is, if any, rare, and it does not play a significant role in the epileptogenicity associated with CCM. On the contrary, blood-brain barrier dysfunction and subsequent astrocytic albumin uptake have been implicated in the epileptogenic mechanism for VM, including CCM and AVM [4, 5].

4.3 | Indistinct neuronal layering in the cerebral cortex adjacent to AVM

The pathogenesis of sporadic AVM remains largely unknown. Most brain AVM are sporadic cases without a clear family history. AVM was mostly considered congenital, but AVM is a dynamic lesion showing de novo formation, growth, spontaneous regression, and recurrence after complete resection [33, 34]. A recent extensive literature review has also suggested that AVM may not be present at birth and may develop later in life until the age of 25 years when the cerebral vasculature becomes mature; i.e., developmental lesions rather than congenital malformations, and AVM formation may involve an interaction between genetic susceptibility or predisposition and environmental or an acquired factors such as a brain tumor, stroke, trauma, inflammation, and other non-specific disorders, i.e., as a second hit [34]. A recent genetic study demonstrated somatic mutations in *KRAS* in 62.5% to 76.2% of a sporadic brain AVM [35, 36], and increased ERK1/2 phosphorylation levels in endothelial cells derived from brain AVM compared to those from normal brain vessels [35]. Besides, *BRAF* V600E and *BRAF* Q636X somatic mutations have also been detected in 4.8% (1 of 21 cases) [36] and 6.3% (1 of 16 cases) [37] of brain AVM, respectively. The results of these studies indicate that somatic mutations in the RAS-MAPK signaling pathway, particularly *KRAS*, may play a significant role as genetic

susceptibility or predisposition in the pathogenesis of sporadic brain AVM. Although it is difficult to determine the precise timing of the AVM formation in the present case, given the well-differentiated pyramidal and polymorphic neurons observed in the white matter in and around the nidus, we hypothesized that the AVM in this patient developed during intrauterine corticogenesis, where it compromised radial migration of neuroblasts. In addition, focal chronic ischemia because of the vascular steal phenomenon secondary to a high flow arteriovenous shunt might suppress the production of neuronal cytoskeletal protein as revealed by NF-H immunohistochemistry, leading to the shrinkage of pyramidal neurons and indistinct cortical layering when examined by NeuN immunohistochemistry.

Furthermore, neuronal hypertrophy in the shallower cortex contributes also to indistinct neuronal layering between L2 and L3. Neuronal hypertrophy could be associated with functional abnormality or hyperexcitability within the local circuit; however, its pathogenesis remains elusive. Our AVM case showed unusual clinicopathological features, as the lesion was initially suspected as a brain tumor but not as vascular malformation, which was the major reason for this patient being treated by epilepsy surgery, and histological examination of the resection specimen revealed the AVM mainly located in the subcortical white matter but not neoplastic lesion. It is extremely rare to obtain the opportunity for histological evaluation of FCD-IIIc adjacent to AVM in the resection specimen from epilepsy surgery because most patients with AVM are treated in the stroke unit. However, further investigation using more AVM cases is needed to characterize FCD-IIIc adjacent to AVM.

4.4 | Histopathologic implications of FCD-IIIc for epileptogenicity

Epileptogenic mechanisms underlying FCD-IIIc are largely unknown [6]. There are currently no reliable histopathological or immunohistochemical markers to confirm epileptogenicity in human tissue samples or animal models. Even among known epileptogenic lesions, only a few developmental lesions [38], including FCD type II [39] and ganglioglioma [40], have convincing experimental evidence for epileptogenicity. Neuronal hypertrophy with aberrant expression of cytoskeletal proteins could be associated with functional abnormality or hyperexcitability within the local circuit. Observing MAP2-positive hypertrophic neurons associated with or without FCD-IIIc is only a weak indicator of epileptogenicity. Region-specific neurophysiological studies are needed for correlation with the histopathological patterns [41].

In conclusion, FCD-IIIc appears to depend on the type of the VM and developmental timing. FCD-IIIc characterized by CPLS represents secondary tissue injury and adaptation during pre- and/or perinatal

development rather than following a pathomechanism independent of LMA-SWS. In patients with LMA-SWS and AVM, FCD-IIIc, characterized by indistinct neuronal layering, seems to represent secondary change associated with altered hemodynamics in the prenatal and postnatal developing cerebral cortex. Further studies will be necessary to address the selective vulnerability of the developing cerebral neocortex in LMA-SWS, including genetic, encephaloclastic, hemodynamic, or metabolic events.

ACKNOWLEDGMENTS

This work was supported in part by a research grant from the Akita Cerebrospinal and Cardiovascular Center. Genetic analysis was performed by Dr. Takuya Furuta (Department of Pathology, Kurume University School of Medicine). We also acknowledge technical assistance provided by Akie Sasamura, Junko Kawamura, Ayaka Suzuki, and Makiko Tanaka (Department of Neuropathology, Research Institute for Brain and Blood Vessels, Akita Cerebrospinal and Cardiovascular Center). Long-term collaborators are Drs. Taku Ochiai (Ochiai Neurological Clinic), Hidetoshi Nakamoto and Satoru Miyao (Epilepsy Center, TMG Asaka Medical Center), and Karl Rössler (Department of Neurosurgery, Medical University of Vienna, Vienna General Hospital).

CONFLICT OF INTEREST

The authors declare that they have no conflicts of interest.

AUTHOR CONTRIBUTIONS

Hajime Miyata and Haruka Kuwashige contributed equally to the original research idea and conception, study design, literature search, data collection, data analysis and interpretation, figure and table formatting, and manuscript drafting. Tomokatsu Hori, Yuichi Kubota, and Tom Pieper provided clinical data and contributed to patient care, including the epileptological evaluation and surgical resection. Hajime Miyata, Roland Coras, Ingmar Blümcke, and Yasuji Yoshida contributed to the neuropathological diagnoses of the surgical specimen. Yasuji Yoshida supervised the study and contributed to critical revision. All authors provided intellectual content and a critical review of the manuscript.

DATA AVAILABILITY STATEMENT

All data provided in this study are available from the corresponding author upon a reasonable requirement.

ORCID

Hajime Miyata  <https://orcid.org/0000-0003-2551-5978>

Yuichi Kubota  <https://orcid.org/0000-0002-6487-2065>

Roland Coras  <https://orcid.org/0000-0001-8617-0913>

Ingmar Blümcke  <https://orcid.org/0000-0001-8676-0788>

REFERENCES

- Challa VR. Vascular malformations and angiomas. In: Kalimo H, editor. Pathology & genetics. Cerebrovascular diseases. Basel: ISN Neuropath Press. 2005; p. 119–24.
- Blumcke I, Spreafico R, Haaker G, Coras R, Kobow K, Bien CG, et al. Histopathological findings in brain tissue obtained during epilepsy surgery. *N Eng J Med*. 2017;377:1648–56.
- Rosenow F, Alonso-Vanegas MA, Baumgartner C, Blümcke I, Carreño M, Gizewski ER, et al. Cavernoma-related epilepsy: review and recommendations for management – report of the Surgical Task Force of the ILAE Commission on Therapeutic Strategies. *Epilepsia*. 2013;54:2025–35.
- Ivens S, Kaufer D, Flores LP, Bechmann I, Zumsteg D, Tomkins O, et al. TGF- β receptor-mediated albumin uptake into astrocytes is involved in neocortical epileptogenesis. *Brain*. 2007;130:535–47.
- Raabe A, Schmitz AK, Pernhorst K, Grote A, von der Brölie C, Urbach H, et al. Cliniconeuropathologic correlations show astroglial albumin storage as a common factor in epileptogenic vascular lesions. *Epilepsia*. 2012;53:539–48.
- Blümcke I, Thom M, Aronica E, Armstrong DD, Vinters HV, Palmini A, et al. The clinicopathologic spectrum of focal cortical dysplasias: a consensus classification proposed by an ad hoc Task Force of the ILAE Diagnostic Methods Commission. *Epilepsia*. 2011;52:158–74.
- Maton B, Kršek P, Jayakar P, Resnick T, Koehn M, Morrison G, et al. Medically intractable epilepsy in Sturge-Weber syndrome is associated with cortical malformation: implications for surgical therapy. *Epilepsia*. 2010;51:257–67.
- Niehusmann P, Becker AJ, Malter MP, Raabe A, Boström A, von der Brölie C. Focal cortical dysplasia type IIIc associates with multiple cerebral cavernomas. *Epilepsy Res*. 2013;107:190–4.
- Engel J Jr., Van Ness P, Rasmussen TB, Ojemann LM. Outcome with respect to epileptic seizures. In: Engel J Jr., editor. Surgical treatment of the epilepsies. 2nd ed. New York: Raven Press; 1993. p. 609–21.
- Shirley MD, Tang H, Gallione CJ, Baugher JD, Frelin LP, Cohen B, et al. Sturge-Weber syndrome and port-wine stains caused by somatic mutation in *GNAQ*. *N Engl J Med*. 2013;368:1971–9.
- Sujansky E, Conradi S. Sturge-Weber syndrome: age of onset of seizures and glaucoma and the prognosis for affected children. *J Child Neurol*. 1995;10:49–58.
- Kossoff EH, Ferenc L, Comi AM. An infantile-onset, severe, yet sporadic seizure pattern is common in Sturge-Weber syndrome. *Epilepsia*. 2009;50:2154–7.
- Cagneaux M, Paoli V, Blanchard G, Ville D, Guibaud L. Pre- and postnatal imaging of early cerebral damage in Sturge-Weber syndrome. *Pediatr Radiol*. 2013;43:1536–9.
- Wang DD, Blümcke I, Coras R, Zhou WJ, Lu DH, Gui QP, et al. Sturge-Weber Syndrome is associated with cortical dysplasia ILAE type IIIc and excessive hypertrophic pyramidal neurons in brain resections for intractable epilepsy. *Brain Pathol*. 2015;25:248–55.
- Vinters HV, Salamon N, Miyata H, Khanlou N, Mathern GW. Neuropathology of developmental disorders associated with epilepsy. In: Engel J Jr., Pedley TA, eds. *Epilepsy: a comprehensive textbook*. 2nd ed. Philadelphia: Lippincott Williams & Wilkins; 2008. p. 137–60.
- Thom M, Eriksson S, Martinian L, Caboclo LO, McEvoy AW, Duncan JS, et al. Temporal lobe sclerosis associated with hippocampal sclerosis in temporal lobe epilepsy: neuropathological features. *J Neuropathol Exp Neurol*. 2009;68:928–38.
- Auer RN. Hypoglycemic brain damage. *Forensic Sci Int*. 2004;146:105–10.
- Tomita N, Nakamura T, Sunden Y, Miyata H, Morita T. Temporal analysis of histopathology and cytokine expression in the rat cerebral cortex after insulin-induced hypoglycemia. *Neuropathology*. 2020;40:240–50.

19. Gil-Nagel A, García Morales I, Jiménez Huete A, Alvarez Linera J, Barrio A, Ruiz Ocaña C, et al. Occipital lobe epilepsy secondary to ulegyria. *J Neurol*. 2005;252:1178–85.
20. Wang D-D, Piao Y-S, Blumcke I, Coras R, Zhou W-J, Gui Q-P, et al. A distinct clinicopathological variant of focal cortical dysplasia IIIc characterized by loss of layer 4 in the occipital lobe in 12 children with remote hypoxic-ischemic injury. *Epilepsia*. 2017;58:1697–705.
21. Whitnall M, Richardson DR. Iron: a new target for pharmacological intervention in neurodegenerative diseases. *Semin Pediatr Neurol*. 2006;13:186–97.
22. Zimmer TS, David B, Broekaart DWM, Schidowski M, Ruffolo G, Korotkov A, et al. Seizure-mediated iron accumulation and dysregulated iron metabolism after status epilepticus and in temporal lobe epilepsy. *Acta Neuropathol*. 2021;142:729–59.
23. Hennekam RC, Biesecker LG, Allanson JE, Hall JG, Opitz JM, Temple IK, et al.; Elements of Morphology Consortium. Elements of morphology: general terms for congenital anomalies. *Am J Med Genet A*. 2013;161A:2726–33.
24. Zafar A, Quadri SA, Farooqui M, Ikram A, Robinson M, Hart BL, et al. Familial cerebral cavernous malformations. *Stroke*. 2019;50:1294–301.
25. Goldstein HE, Solomon RA. Epidemiology of cavernous malformations. *Handb Clin Neurol*. 2017;143:241–7.
26. Labauge P, Denier C, Bergametti F, Tournier-Lasserre E. Genetics of cavernous angiomas. *Lancet Neurol*. 2007;6:237–44.
27. Petersen TA, Morrison LA, Schrader RM, Hart BL. Familial versus sporadic cavernous malformations: differences in developmental venous anomaly association and lesion phenotype. *Am J Neuroradiol*. 2010;31:377–82.
28. McDonald DA, Shi C, Shenkar R, et al. Lesions from patients with sporadic cerebral cavernous malformations harbor somatic mutations in the CCM genes: evidence for a common biochemical pathway for CCM pathogenesis. *Hum Mol Genet*. 2014;23:4357–70.
29. Cutsforth-Gregory JK, Lanzino G, Link MJ, Brown RD Jr, Flemming KD. Characterization of radiation-induced cavernous malformations and comparison with a nonradiation cavernous malformation cohort. *J Neurosurg*. 2015;122:1214–22.
30. Hashimoto H, Sakaki T, Ishida Y, Shimokawara T. Fetal cavernous angioma—case report. *Neurol Med Chir (Tokyo)*. 1997;37:346–9.
31. Henrich W, Stupin JH, Bühling KJ, Bühner C, Bassir C, Dudenhausen JW. Prenatal sonographic findings of thalamic cavernous angioma. *Ultrasound Obstet Gynecol*. 2002;19:518–22.
32. Blümcke I, Coras R, Busch RM, Morita-Sherman M, Lal D, Prayson R, et al. Toward a better definition of focal cortical dysplasia: an iterative histopathological and genetic agreement trial. *Epilepsia*. 2021;62:1416–28.
33. Thomas JM, Surendran S, Abraham M, Rajavelu A, Kartha CC. Genetic and epigenetic mechanisms in the development of arteriovenous malformations in the brain. *Clin Epigenetics*. 2016;8:78.
34. Tasiou A, Tzerefos C, Alleyne CH, Boccardi E, Karlsson B, Kitchen N, et al. Arteriovenous malformations: congenital or acquired lesions? *World Neurosurg*. 2020;134:e799–807.
35. Nikolaev SI, Vetiska S, Bonilla X, Boudreau E, Jauhainen S, Rezai Jahromi B, et al. Somatic activating KRAS mutations in arteriovenous malformations of the brain. *N Engl J Med*. 2018;378:250–61.
36. Hong T, Yan Y, Li J, Radovanovic I, Ma X, Shao YW, et al. High prevalence of KRAS/BRAF somatic mutations in brain and spinal cord arteriovenous malformations. *Brain*. 2019;142:23–34.
37. Goss JA, Huang AY, Smith E, Konczyk DJ, Smits PJ, Sudduth CL, et al. Somatic mutations in intracranial arteriovenous malformations. *PLoS One*. 2019;14:e0226852.
38. Blümcke I, Budday S, Poduri A, Lal D, Kobow K, Baulac S. Neocortical development and epilepsy: insights from focal cortical dysplasia and brain tumours. *Lancet Neurol*. 2021;20:943–55.
39. Koh HY, Jang J, Ju SH, Kim R, Cho G-B, Kim DS, et al. Non-cell autonomous epileptogenesis in focal cortical dysplasia. *Ann Neurol*. 2021;90:285–99.
40. Koh HY, Kim SH, Jang J, Kim H, Han S, Lim JS, et al. BRAF somatic mutation contributes to intrinsic epileptogenicity in pediatric brain tumors. *Nat Med*. 2018;24:1662–8.
41. Rampp S, Rössler K, Hamer H, Illek M, Buchfelder M, Doerfler A, et al. Dymorphic neurons as cellular source for phase-amplitude coupling in Focal Cortical Dysplasia Type II. *Clin Neurophysiol*. 2021;132:782–92.

How to cite this article: Miyata H, Kuwashige H, Hori T, Kubota Y, Pieper T, Coras R, et al. Variable histopathology features of neuronal dyslamination in the cerebral neocortex adjacent to epilepsy-associated vascular malformations suggest complex pathogenesis of focal cortical dysplasia ILAE type IIIc. *Brain Pathology*. 2022;32:e13052. <https://doi.org/10.1111/bpa.13052>